Appl. Phys. B 61, 569–579 (1995)

Applied Physics B Lasers and Optics

Continuous-wave mode-locked solid-state lasers with enhanced spatial hole burning

Part II: Theory

F.X. Kärtner, B. Braun, U. Keller

Swiss Federal Institute of Technology, Institute of Quantum Electronics, ETH Hönggerberg HPT, CH-8093 Zürich, Switzerland (Fax: + 41-1/633-1059, E-mail: KAERTNER@iqe.ethz.ch)

Received: 12 April 1995/Accepted: 8 June 1995

Abstract. In Part I of this paper [1] experimental results were presented and discussed. In this part, we investigate theoretically the dynamics of end-pumped solid-state lasers due to enhanced spatial hole burning. This becomes possible by a fast numerical implementation of the saturated gain in the presence of strong spatial hole burning that allows to treat the multimode case for an arbitrary pumping level. We find for a wide range of laser parameters that the mode spacing of the cw running modes is essentially determined by the length of the gain medium and only weakly depends on the absorption depth of the pump transition. It is shown that spatial hole burning can lead to a completely flat saturated gain profile over half of the gain bandwidth. In mode-locked lasers, the flat gain due to spatial hole burning results in shorter pulses. But the pulses are neither Gaussian-nor sech-shaped as they are in actively or passively mode-locked lasers without spatial hole burning. Further, we show that soliton-like pulse shaping can be used to restore a transform-limited sech-shaped pulse in an end-pumped solid-state laser while exploiting the full gain bandwidth of the laser material.

PACS: 42.60; 42.55; 42.65

Most of the existing laser theories covering the influence of Spatial Hole Burning (SHB) on the laser dynamics are limited to pumping close above threshold or single-mode operation [2–5]. Some of the effects due to SHB can then be described analytically. As early as 1963, Tang et al. [2] realized that multimode oscillation of a laser with homogeneously broadened gain material is due to SHB. They derived a formula based on rate equations which gives the number of oscillating modes for a given pump power, assuming that the pumping level is slightly above threshold and that the cavity is completely filled with the gain material [2]. Sargent describes the SHB in terms of Bragg-like gratings induced by the standing wave [3]. For the analytical discussion he also expands the inversion up to first order in the mode intensities, which again is only valid for pumping close to threshold [3, 6]. Zayhowski treats SHB by starting with one single lasing mode and looking at the gain experienced by the other modes in the presence of the first one, resulting in a condition for single-mode operation and a prediction of the next running mode [4]. A similar approach is presented by Kintz and Baer [5]. The influence of SHB on pulse shortening in a mode-locked laser is also treated by Flood et al. [7]. Their analysis is based on a gain grating model developed for investigation of pulse shortening in colliding-pulse mode-locked dye lasers by Stix and Ippen [8]. However, in [8], a slowly varying sinusoidal gain grating is assumed, and that does not correctly describe the non-sinusoidal gain grating of a solid-state laser pumped many times (≈ 100) above threshold. Recently, Fu and Haken [9] have extended the early work of Haken and Sauermann considering mostly the frequency-pushing and pulling effects due to SHB in the single- and two-mode case [10–12] to the multimode cw operation for large pump levels. However, they considered the case of a short cavity completely filled with gain and they did not consider the mode-locked case.

The paper is organized as follows. In Sect. 1, we implement the optical gain for arbitrary pumping levels and especially for the gain medium at the end of the cavity, making extensive use of the Fast Fourier Transformation (FFT). With this expression for the gain, we study in the following Sect. 2–5 the laser dynamics when operating cw, actively as well as passively mode-locked, with and without Self-Phase Modulation (SPM) occuring in the gain medium, respectively. As we will see, the pulses show a large time–bandwidth product due to SHB. Therefore, in Sect. 6, we demonstrate theoretically that transform-limited pulses can be generated by employing soliton-like pulse shaping due to negative Group-Velocity Dispersion (GVD) and SPM. We apply the theory to end-pumped Nd:YLF and Nd:LSB lasers, showing by simulations that these lasers should be able to generate almost transform-limited sech-shaped pulses of about 1.7 ps and 400 fs pulse width, respectively.

1 The optical gain in end-pumped lasers

In this section, we rederive the optical gain in an end-pumped solid-state laser to clarify notation and approximations used in the following, despite the fact that similar equations have been derived in many of the works cited above. The basis for the theory is the simplified laser model shown in Fig. 1. We assume that the only lasing transverse mode is a TEM_{00} mode. Thus, the transverse field distribution in the gain medium with length l_g and refractive index n_r is Gaussian with a waist w_L and effective area $A_{\text{eff,gain}} = \pi w_L^2$, if the gain medium is shorter than the confocal parameter of the beam. The remaining length of the total cavity is l_{cav}. Since all the intensity-dependent effects in the laser, such as amplification and SPM, occur in the gain medium, we can treat the laser as if the transverse mode profile was constant over the full cavity length. If we assume perfectly reflecting cavity mirrors, we can decompose the longitudinal field distribution of the transverse electric field, polarized in x-direction, by a complete set of modes:

$$\mathbf{E}(x, y, z, t) = E(z, t, T)\, u(x, y)\, \mathbf{e}_x,$$

with

$$u(x, y) = \exp\left(-\frac{x^2 + y^2}{w^2}\right),$$

$$E(z, t, T) = \frac{2^{3/2}}{\sqrt{c\varepsilon}} \sum_m [A_m(T)\, e^{-i\omega_m t} + \text{c.c.}] \sin[k_m(z)\, z], \quad (1)$$

and

$$k_m(z) = \begin{cases} m \dfrac{\pi}{l_{\text{opt,tot}}}\, n_r; \; for \;\; 0 < z < l_g \\ m \dfrac{\pi}{l_{\text{opt,tot}}}; \; for \;\; l_g < z < l_g + l_{\text{cav}} \end{cases}. \quad (2)$$

Here, $l_{\text{opt,tot}} = n_r l_g + l_{\text{cav}}$ is the total optical length of the cavity and ε the dielectric constant of the undoped gain material, so that $|A_m|^2$ is proportional to the average intensity over the cross section of the m-th longitudinal mode travelling in one direction. Note that we have introduced the space-dependent wave numbers $k_m(z)$ to account for the different refractive index in the gain medium and the rest of the cavity, but neglected the reflections at this intracavity surface since in the real cavity the gain medium is placed at Brewster's angle. The amplitudes of the field modes are time dependent, and we assume that the time evolution can be decomposed into a fast oscillation at the cold-cavity resonance frequencies $\omega_m \approx k_m c$, i.e., without the active laser ions, and into slowly varying amplitudes that only change appreciably over many cavity round-trip times $T = nT_R$, where $T_R = 2l_{\text{opt,tot}}/c$ is the round-trip time for the light in the cold cavity. Thus, T is a coarse-grained time on the order of the round-trip time in the cavity, whereas t is the fast time which is on the order of the optical period of oscillation. The active laser ions are described as equivalent quantum mechanical two-level systems. The interaction of the active laser ions doped into the laser crystal with the multimode electromagnetic field can then be described by the semiclassical Maxwell-Bloch equations within the rotating-wave approximation [6, 12]:

$$\frac{\partial}{\partial t} P^{(+)}(z, t, T) = -(\gamma + i\omega_0) P^{(+)} + igW E^{(+)}, \quad (3a)$$

$$\frac{\partial}{\partial T} W(z, T) = -\frac{W - W_0(z)}{\tau_L} + \frac{1}{T_R} \int_0^{T_R} (ig^* P^{(+)} E^{(-)} + \text{c.c.})\, dt, \quad (3b)$$

$$T_R \frac{\partial}{\partial T} A_m(T) = -l A_m(T) + \frac{\omega_0}{4i\sqrt{c\varepsilon}} \frac{1}{T_R(l_g + l_{\text{cav}})} \times \int_0^{T_R} e^{i\omega_m t} \int_0^{l_g} P^{(+)}(z, t, T) \sin(k_m z)\, dz\, dt. \quad (3c)$$

Here, P describes the electric polarization in the gain medium, W the saturated inversion averaged over one roundtrip, W_0 the unsaturated inversion created by optical pumping, ω_0 the transition frequency between the laser levels, τ_L the upper state lifetime; γ is the dipole decay rate, which is related to the gain bandwidth by $\gamma = \pi A f_g$, g the coupling coefficient between the laser light and the atoms providing the gain and l the cavity losses. The superscript $^{(\pm)}$ denotes as usual, the positive and negative frequency parts of the electric field and polarization proportional to $e^{\mp i\omega t}$, respectively.

For solid-state lasers, the interaction cross section, i.e., the coupling constant g, is rather small, and usually the pulse energy is several orders of magnitude smaller than the saturation energy of the gain medium, so that pulse shaping due to gain saturation can be neglected. Therefore, the inversion only changes over many round trips of the laser light in the cavity, i.e., $W = W(z, T)$. This also means that only a whole series of pulses saturate the laser gain considerably if the laser is mode-locked. Representing the polarization by a Fourier series similar to (1)

$$P(z, t, T) = \sum_m [P_m^{(\pm)}(T) e^{-i\omega_m t} + \text{c.c.}] \sin(k_m z), \quad (4)$$

we obtain from (3a)

$$P_m^{(+)}(T) = \frac{2^{3/2} ig}{\sqrt{c\varepsilon}} \frac{W(z, T)}{[\gamma + i(\omega_0 - \omega_m)]} A_m(T). \quad (5)$$

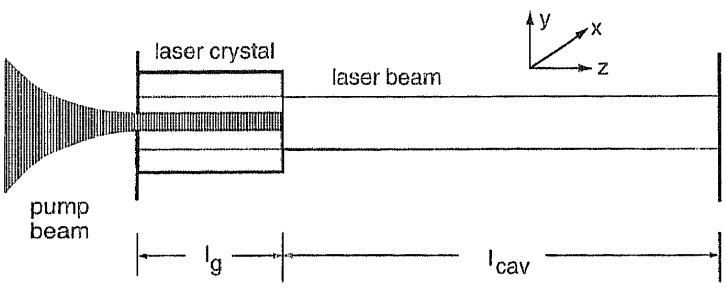

Fig. 1. Scheme of an end-pumped solid-state laser cavity. We assume a constant Gaussian-shaped transverse field distribution and do not consider any reflections at the boundary to the gain medium since the medium is at the Brewster angle in a real cavity

Back substitution into (3b) and (3c) and averaging over one round-trip time in the fast variable t results in the equations of motion for the slowly varying mode amplitudes

$$T_R \frac{\partial}{\partial T} A_m(T) = -l A_m(T) + \frac{\omega_0 |g|^2}{2(l_g + l_{cav})\varepsilon} \frac{\int_0^{l_g} W(z,T) \sin^2(k_m z)\, dz}{[\gamma + i(\omega_0 - \omega_m)]} A_m(T) \tag{6a}$$

and inversion

$$\frac{\partial}{\partial T} W(z,T) = -\frac{W - W_0(z)}{\tau_L} - W \sum_{m=0}^{\infty} L(\omega_0 - \omega_m) \times \frac{8|A_m|^2}{E_L} \sin^2(k_m z), \tag{6b}$$

where $E_L = \gamma c \varepsilon / 2|g|^2 = \hbar\omega_0/\sigma$ is the saturation fluence of the gain medium, which can also be expressed by the gain cross section σ; $L(\omega)$ is the Lorentzian line profile of the homogeneously broadened laser transition:

$$L(\omega) = \frac{\gamma^2}{\gamma^2 + \omega^2}. \tag{7}$$

Here, we implicitly assumed that the laser gain saturates homogeneously with the peak intensity of the Gaussian beam, which is a good approximation for the Ti : Sapphire end-pumped lasers in [1], since the pump spot in the laser crystal is much smaller than the beam size of the laser mode (Fig. 1). This has to be modified with an effective saturation fluence for diode-pumped lasers where the pump spot is usually as large as the laser mode itself.

In the following, we are concerned with the steady-state solutions of the differential equations (6a, b). We obtain from (6b) for the steady-state inversion

$$W(z,T) = \frac{W_0(z)}{1 + \frac{8}{I_L} \sum_m |A_m(T)|^2 L(\omega_0 - \omega_m) \sin^2(k_m z)}, \tag{8}$$

where I_L is the saturation intensity

$$I_L = \frac{\gamma c \varepsilon}{2\tau_L |g|^2} = \frac{\hbar\omega_0}{\sigma\tau_L}. \tag{9}$$

The total amplitude gain $g(\omega_n)$ seen by the n-th mode is according to (6a) given by the overlap integral of the field intensity with the inversion multiplied by the line profile and a normalization constant C_0:

$$g(\omega_n) = C_0 L(\omega_0 - \omega_n) \int_0^{l_g} W(z,T) \sin^2(k_n z)\, dz. \tag{10}$$

In the steady state, the round-trip gain g equals the total losses l of the cavity. Introducing the pump parameter r, which is the ratio between the actual pump power and the pump power when the first mode reaches threshold, and taking into account the exponential decay of the longitudinal pump field, we arrive with (8) and (10) at the final steady-state equation for the normalized gain:

$$g(\omega_n) = r l L(\omega_0 - \omega_n) \frac{2\alpha}{1 - e^{-\alpha l_g}} \times \int_0^{l_g} \frac{e^{-\alpha z} \sin^2(k_n z)\, dz}{1 + 8 \sum_m L(\omega_0 - \omega_m) \frac{|A_m|^2}{I_L} \sin^2(k_m z)}. \tag{11}$$

Here, α is the absorption coefficient of the pump transition, and the normalization is chosen such that for $r \equiv 1$ the first mode (at line center) starts lasing. In this paper, we restrict ourselves to the steady-state behavior of the cw running and cw model-locked laser and are not so much interested in transient phenomena or Q-switching of the laser. Therefore, we derive an effective equation of motion for the field amplitudes by substitution of the steady-state gain (11) into (6a), i.e., we adiabatically eliminate the inversion [13]:

$$T_R \frac{\partial}{\partial T} A_m(T) = -l A_m(T) + [1 - i(\omega_0 - \omega_m)] \times G(\omega_m) A_m(T). \tag{12}$$

One has to be careful with the physical interpretation of the solutions of (12). It only correctly describes the real field dynamics over time if the field amplitudes do not change too much on a time scale shorter than the upper-state lifetime. This will be the case for the build-up of the cw lasing pattern that evolves on a rather long time scale, as will be seen in the next section. However, if the simulation of (12) with (8) leads to a steady-state solution, we have found a steady-state solution of the full system (6a, b) self-consistently.

2 The cw lasing mode pattern

For the time evolution of the mode intensities $I_m = |A_m|^2$ we obtain from (16)

$$T_R \frac{\partial}{\partial T} I_m = 2[g(\omega_m) - l] I_m. \tag{13}$$

The cw running modes and their stationary intensities are determined by the zeros of the right-hand side of (13). Usually, this gives one a set of some hundred coupled nonlinear equations with little hope for an analytical solution. Even a direct numerical solution of this problem as a function of the pump parameter is rather difficult. Therefore, we used an integration routine to integrate (13) numerically until the steady state is reached. We used the GEAR method [14], well known in the simulation of electronic circuits, since the set of differential equations (13) is very stiff, i.e., the dynamics in the system occurs on time scales that differ by orders of magnitude, and the integration time until the steady state is reached is rather long. The numerical implementation of the saturated gain (11) is discussed in the Appendix. The number of modes N which have to be considered depends on the gain

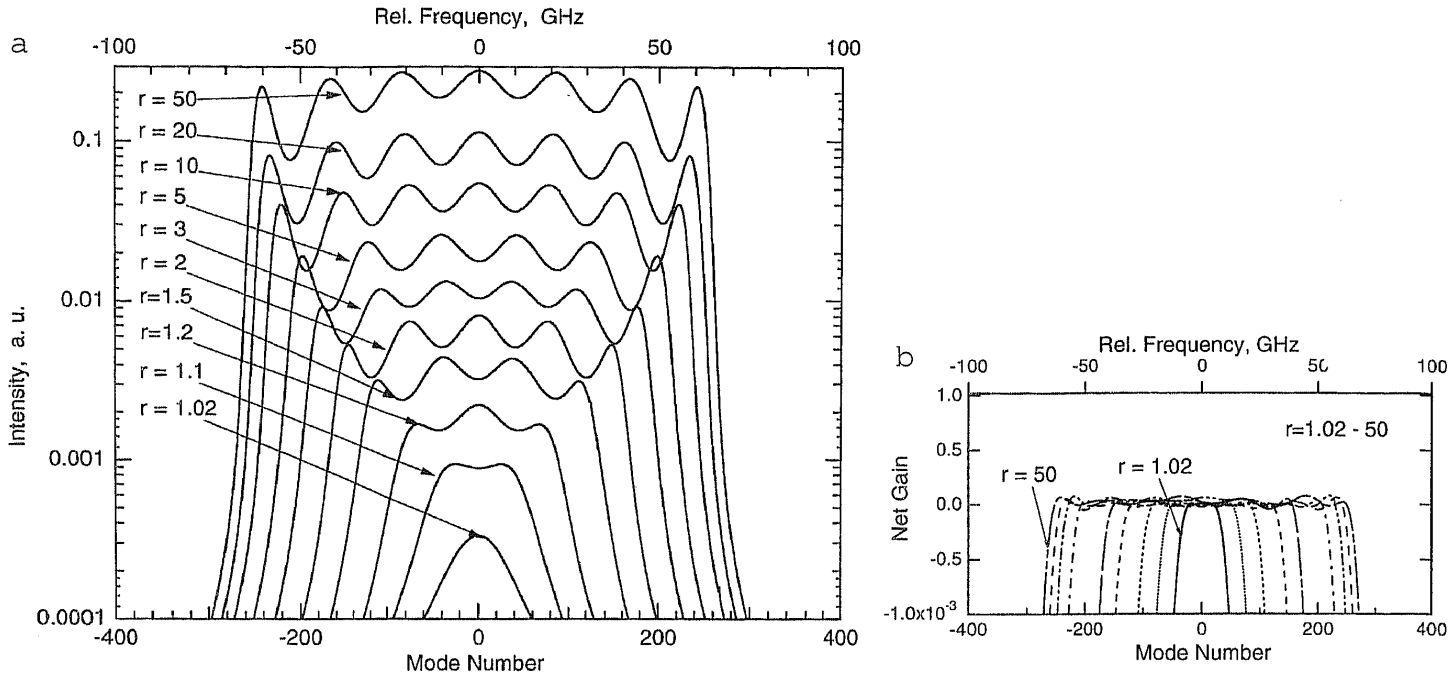

Fig. 2. a Intensity distribution in the modes of the end-pumped Nd:YLF laser of [1]. The simulation starts from a constant intensity distribution over the modes. The distributions shown are reached after simulation of 30000 cavity decay times for various pump parameters r. **b** Net gain according to (15) for the intensity patterns in **a**

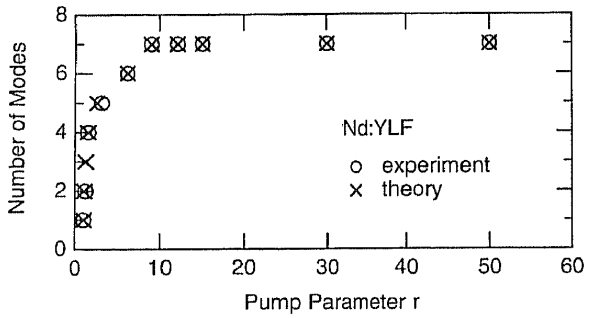

Fig. 3. Calculated and measured number of cw lasing modes in the end-pumped Nd:YLF laser of [1]

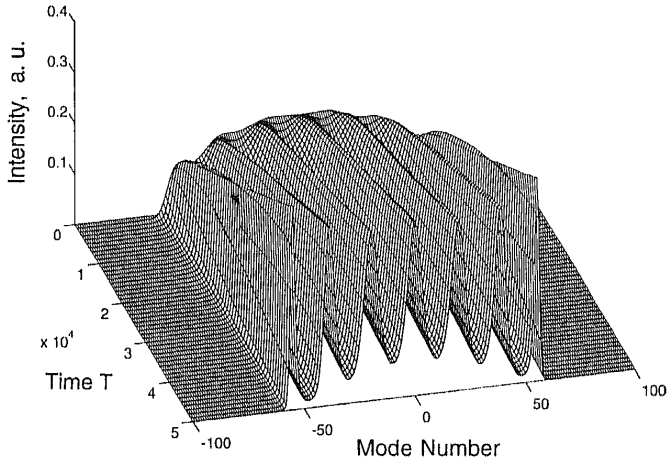

Fig. 4. Simulation of the build-up of the cw lasing pattern from noise shown over 50000 cavity decay times, i.e. 6 ms real time

bandwidth and the cavity round-trip frequency. In the case investigated experimentally in [1], we had a Gain-at-the-End (GE) cavity with a typical repetition rate of $f_R = 250$ MHz and a Nd:YLF laser crystal. The model parameters determining the mode spacing of the cw lasing modes were $l_g = 4.5$ mm, $l_{cav} = 59.3$ cm, $\Delta f_g = 360$ GHz, $n_r = 1.47$, $\alpha = 1/2.3$ mm and the other parameters were $l = 0.02$, $I_L = 2.3$ kW/cm^2. CW laser action occurred over almost half of the gain bandwidth. Thus, we have to consider at least $N = \Delta f_g/f_R \approx 700$ modes. In Fig. 2a, the results for the GE cavity with a Nd:YLF crystal as gain material are shown for different pump parameters and simulation of 800 modes central to the peak of the gain. The mode intensity distribution is plotted after the laser has been simulated for 30000 τ_c for each value of the pump parameter, where $\tau_c = T_R/2l$ is the cavity decay time. The results are independent of the initial values of the mode intensities. Note that the intensity patterns are plotted on a logarithmic scale in contrast to the measured distributions shown in Fig. 6 of [1]. In Fig. 3, the calculated number of lasing modes as a function of the pump parameter is compared with the experiment. The agreement between experiment and theory is excellent with respect to the number of modes running at a given pump level. Thus, the simplified laser model is so far a good match to the real laser.

Figure 4 shows the simulated mode pattern for the Nd:YLF laser with the parameters over a time span of 50000 cavity decay times corresponding to 6 ms real time. After 10000 cavity decay times, the spacing between the modes does not change any further. However, suppression of neighboring modes occurs on a rather long time scale; it takes many upper-state lifetimes. The rather long build-up time of the cw lasing mode pattern also explains why

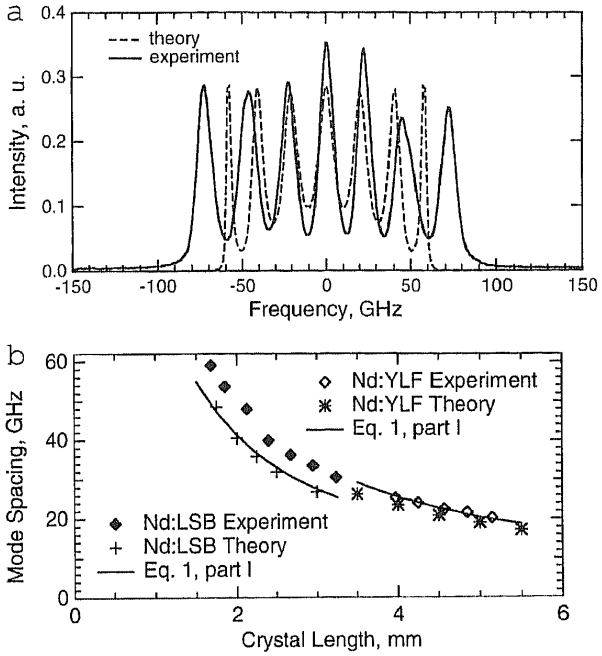

Fig. 5. **a** Measured and calculated cw lasing mode pattern for the Nd:YLF laser of [1] at a pump parameter $r = 50$. **b** Average spacing of the lasing modes for the Nd:YLF and Nd:LSB laser for different crystal lengths

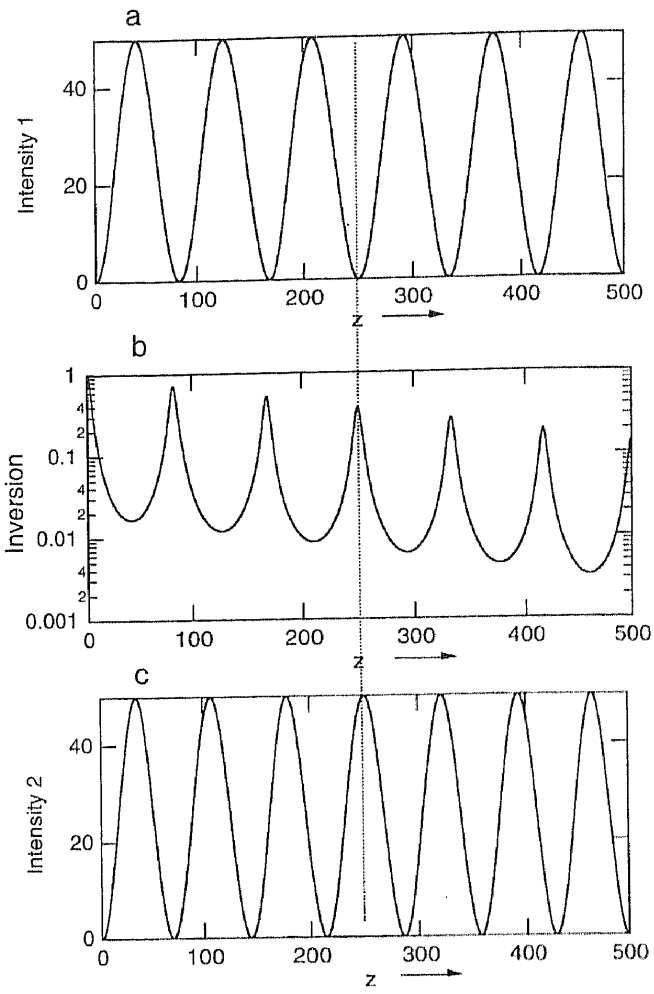

Fig. 6. **a** Normalized intensity distribution of the standing wave in the gain medium when one mode is running for $r = 50$ (drawn not to scale). **b** Corresponding inversion. **c** Intensity distribution of the next running mode which has the largest overlap with the unsaturated inversion due to the first two modes running

the pattern is less distinct for unstable laser performance, as has been observed in the experimental part, too. The reason for the long build-up time can be inferred from Fig. 2b, which shows the net gain, i.e., the saturated gain according to (11) minus loss, for the cw lasing patterns in Fig. 2a. The net loss between the lasing modes is very small and therefore, the suppression of neighboring modes takes many thousands of cavity decay times. Thus, the long build-up time of the cw lasing pattern is a consequence of the extreme SHB-induced flattening of the saturated gain.

For a pump power fifty times above threshold ($r = 50$) seven modes are lasing with an average calculated mode spacing of 21 GHz between each mode from the numerical simulation, which is in good agreement with the calculated value of 23 GHz from the simple Eq. (1) of [1] and the measured value of 23 GHz. Figure 5a shows a detailed comparison of the computed and measured cw spectrum for the Nd:YLF laser. We see that the calculated mode spacing is somewhat smaller than the measured one and that the difference between the calculated and measured mode spacing of the outer modes is larger. However, taking into account a 5% error in the actual gain length and of up to 20% error in the gain bandwidth of the homogenously broadend transition for different pumping levels as shown in [1], the agreement between experiment and theory is satisfactory, since the errors in the mode spacing add up from the inner to the outer modes.

The average mode spacing as a function of the gain length for different absorption parameters and the measurements for Nd:YLF and Nd:LSB with the laser parameters $l_g = 2.5$ mm, $l_{cav} = 59.3$ cm, $\Delta f_g = 1100$ GHz, $n_r = 1.82$, $\alpha = 1/280$ µm and $l = 0.02$, $I_L = 12.4$ kW/cm^2 for the latter are shown in Fig. 5b, together with the experimental results and the simplified mode spacing given by (1) of [1]. It is interesting to note that the mode spacing is still mainly determined by l_g, even with an absorption length of about one-tenth of the total crystal length. The reason for this suprising result is clarified by Figs. 6 and 7. In Fig. 6a, we have plotted the field intensity of one running mode and underneath, in Fig. 6b, the steady-state inversion which is burned into the gain medium according to (8) for one mode lasing with $4I/I_L = 50$. We see that the intensity pattern of the second mode, which starts to lase according to (1) of [1] (Fig. 6c), is exactly in phase with the inversion in the middle of the gain medium. By this choice of the second-mode frequency, the mode pattern and the inversion stay in phase over the longest possible distance in the gain medium. This maximizes the overlap integral of the intensity pattern of mode 2 with the inversion, which results in maximum gain for mode 2 (10). Then, both modes are running and, since they are strongly coupled with each other via SHB, they run with equal power, as seen in the experiment. Figure 7a shows the new intensity distribution and Fig. 7b the corresponding inversion in the gain medium with the two modes running. Figure 7c gives the intensity pattern of the next running mode according to (1) of [1].

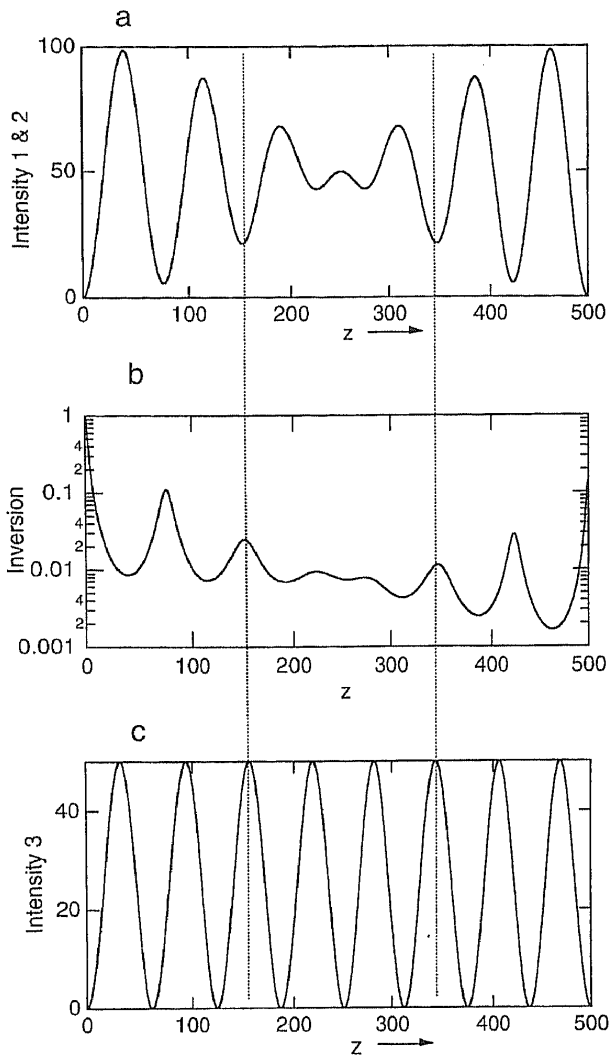

Fig. 7a–c. Normalized intensity distribution (**a**) of the standing wave in the gain medium when the first two modes shown in (**a**) and (**c**) are running; (**b**) corresponding inversion and (**c**) intensity distribution of the third lasing mode that has the largest overlap with the unsaturated inversion due to the first two modes running

This mode has now the most overlap with the remaining inversion and therefore starts to lase next. When pumping many times above threshold, the peaks in the inversion are very sharp. To maximize the overlap integral, it is necessary that the next mode which starts to lase is exactly in phase with the gain grating over the longest possible distance which leads to the simple Eq. (1) of [1]. The exponential decay of the inversion due to optical pumping of the gain is therefore of less importance. This observation explains why the mode spacing is much more sensitive to the length of the gain medium than to the absorption depth of the pump light, as long as they differ not more than an order of magnitude.

3 Active mode locking with enhanced SHB

In the following, we are only interested in the steady-state pulse shapes and spectra. Since the gain medium does not saturate within one pulse, there is no pulse shaping due to gain saturation, and according to (12), we obtain for the change in the spectrum after one round trip due to the net gain, i.e., saturated gain minus loss:

$$A_m^{\mathrm{G}}(T+T_{\mathrm{R}}) = \exp[-l+[1-\mathrm{i}(\omega_0-\omega_m)/\gamma] \times g(\omega_m)]\, A_m(T)\,. \tag{14}$$

Here, the gain is also evaluated using $A_m(T)$ since we assume small changes per round trip. Thus, (14) is equivalent to an Euler step in the integration of (12) over one round trip. The change in the field per round trip due to an Acousto-Optic Modulator (AOM) can easily be described in the time domain:

$$A(T,t) = \sum_{m=0}^{N} A_m(T)\exp[-\mathrm{i}(\omega_m-\omega_0)t]\,. \tag{15}$$

An AOM with modulation depth M driven exactly at the cavity round-trip frequency $\omega_{\mathrm{M}} = 2\pi/T_{\mathrm{R}}$ couples energy from one mode to neighboring modes that can be modelled by the map [15, 16]:

$$A^{\mathrm{M}}(T+T_{\mathrm{R}},t) = \exp\{-M[1-\cos(\omega_{\mathrm{M}}t)]\}\; A(T,t)\,. \tag{16}$$

Note that the steady-state pulses are much shorter than the cavity round-trip time. Therefore, the detailed shape of the modulation function in (16) is not important, but only the curvature at $t=0$, which accounts for pulse shape and pulsewidth. Since the change in the pulse shape close to steady-state is rather small per round trip, we can compute the steady state by alternating application of (14) to (16), called the split-step-Fourier method. However, simulation of this set of equations does not lead to a stationary state, since the mode spacing of the cold cavity is not equal to the mode spacing of the cavity filled with the pumped gain medium. This leads to a detuning of the modulation frequency from the round-trip frequency of the pulse in the pumped cavity that prevents mode locking. Of course, the experimenter adjusts the drive frequency of the modulator to the actual round-trip frequency of the laser to obtain the shortest pulses. To account for this effect in the theory, we have to reinterpret the mode spacing in (14) as that of the warm cavity or simply subtract the average group delay that the pulse experiences when passing the gain medium

$$\frac{1}{\tau_{\mathrm{g}}} = \frac{g(\omega_0)}{\gamma}\,. \tag{17}$$

Here, we implicitly assumed that the pulse runs at the center of the gain line. Figures 8a, b show the steady-state pulse shapes and spectra after simulation of 500 000 cavity round trips for a modulation depth in the interval $0.1 \le M \le 1$, a pump parameter $r = 200$ and amplitude losses $l = 0.02$ estimated for the Nd : YLF laser in [1]. The steady-state pulses and spectra are non-Gaussian in contrast to a homogeneously broadened laser without SHB [15], as observed in [1]. Furthermore, we can see that the full spectrum is not completely locked if the mode-locker is too weak, i.e., $M \le 0.1$. As shown by Fig. 8c, the FWHM pulsewidth obtained is 6 ps, independent of the modulation depth for $0.1 \le M \le 1$. The steady-state net gain, i.e., the difference between saturated gain g and cavity loss l, extracted from the simulation is shown in Fig. 8d. The net gain also shows no dependence on the

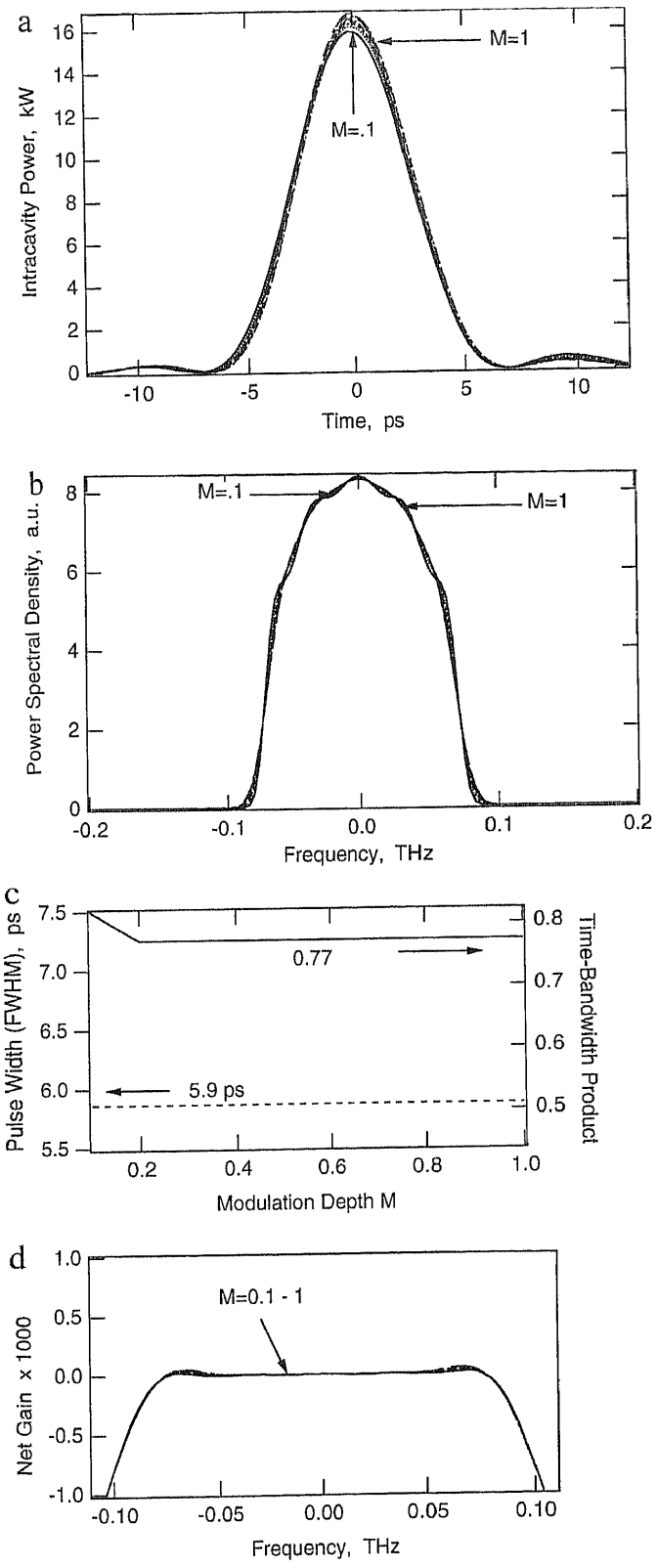

Fig. 8a–d. Simulation of an end-pumped Nd:YLF laser actively mode-locked with an AOM for various modulation depths and $r = 200$: (**a**) Steady-state pulse shapes after 500 000 cavity round-trips, (**b**) corresponding power spectral densities, (**c**) time–bandwidth product and pulsewidth as a function of the modulation depth and (**d**) saturated net gain per round trip

modulation depth. The flat gain in the GE cavity leads to shorter pulses at the same modulation depth than a Gain-in-the-Middle (GM) cavity with negligible SHB. But the pulses are not any longer Gaussian and therefore, the time–bandwidth product is not 0.441, but roughly 0.8 (Fig. 8c), close to the time–bandwidth product observed in the experiment (Fig. 9c of [1]). Due to the flat gain, the pulse spectra are more of a square shape. The Fourier transform of a square pulse is a sinc function. Therefore, the pulses do show wings in the leading and trailing edge of the pulse. These general features of the pulse in mode-locked end-pumped solid-state lasers have been observed directly in the experiments by Sweetser et al. [17] performing a cross-correlation measurement with a femtosecond dye laser.

However, the effects shown in Fig. 8 are blurred in the experiment because the laser is strongly focused in the gain material to obtain large gain. This strong focusing leads to a weak SPM of the pulse. The weak SPM can be large enough to be comparable with the modulation due to the active modulator in the steady state and therefore leads to a deformation of the spectrum that can run the laser even unstable at a weak modulation depth [16].

4 Active mode locking with enhanced SHB and SPM

To solve the pulse dynamics with SPM, we have to add the changes in pulse shape per round trip due to SPM by multiplication with the instantaneous phase shift due to the intensity-dependent refractive index

$$A^{\mathrm{SPM}}(T + T_{\mathrm{R}}, t) = A(T, t)\exp[\mathrm{i}\delta|A(T, t)|^2], \tag{18}$$

where $\delta = (2\pi/\lambda)n_2\, 2l_{\mathrm{g}}$ is the SPM coefficient for the laser beam per round trip due to the double pass through the laser crystal in the linear cavity. The intensity-dependent index change in Nd:YLF is $n_2 = 1.43 \times 10^{-16}$ cm^2/W [1] and therefore, we obtain for the Nd:YLF laser $\delta = 8$ cm^2/TW. Figures 9a, b show the steady-state solutions in the spectral and time domain for the simulation of (15)–(18) which includes the effects due to SHB and SPM for a mode size of $A_{\mathrm{eff,gain}} = 22\,000\ \mu\mathrm{m}^2$ in the Nd:YLF crystal and the other parameters as in Sect. 3. If the modulation depth is too weak, as is the case here for $M < 0.1$, the simulation does not reach a steady state within the simulated 500 000 cavity round trips for each value of the modulation depth. This is a well-known behavior due to SPM, as already shown by Haus and Silberberg [18] for lasers without SHB. With SHB, the tendency to instability is even increased because the flattened gain cannot reduce the SPM-induced chirp by gain filtering. This also leads to an increased sensitivity of the laser to detuning between modulation period and round trip time, which was observed during the experiments in [1]. Since the actual detuning in the experiment is not known, we always retimed the pulse maximum to the minimum loss point of the modulator in the simulation. Figure 9c shows the computed pulsewidth and the time–bandwidth product as a function of the modulation depth. We see the increase in pulsewidth and time bandwidth product for small modulation depth, until the pulse formation no longer becomes stationary over the time span simulated. The spectra develop a characteristic side lobe (Fig. 9b) that is also seen in the experiment (Fig. 5 of

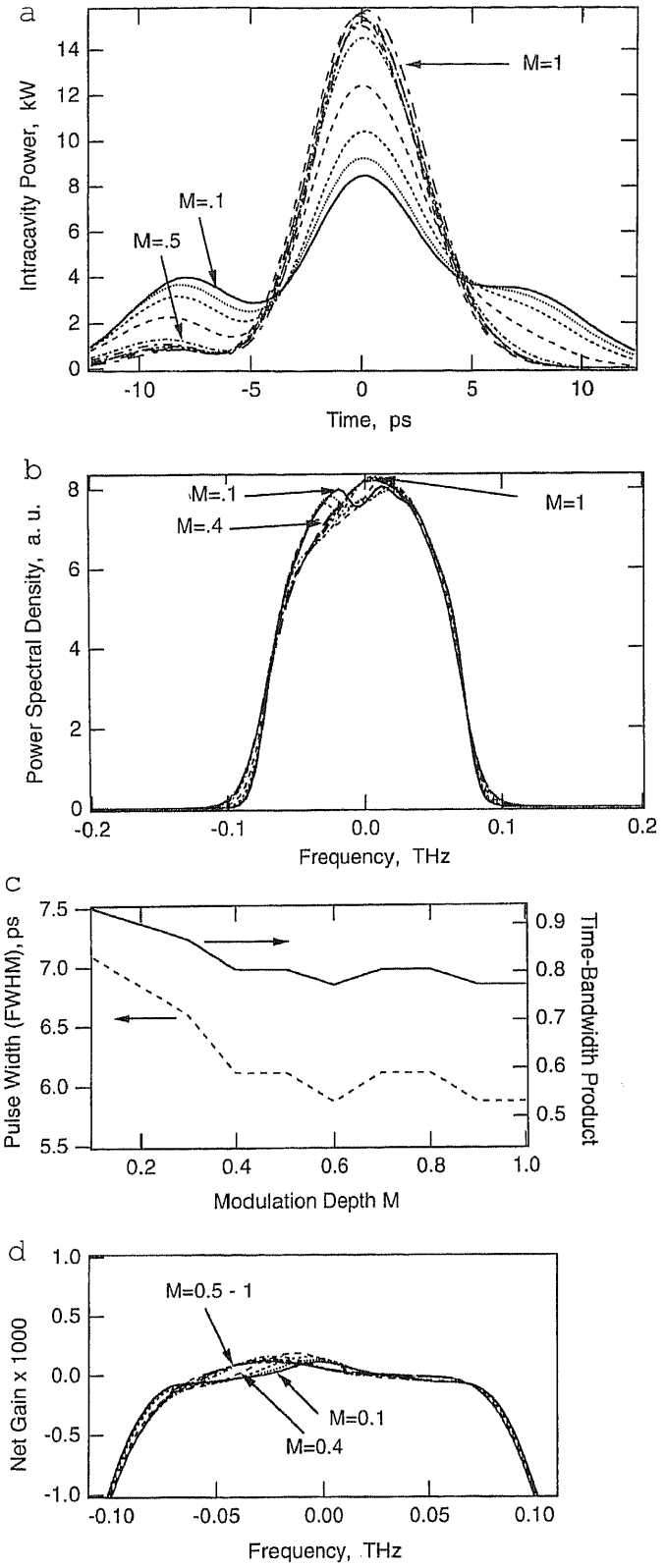

Fig. 9a–d. Simulation of an end-pumped Nd:YLF laser actively mode-locked with an AOM and SPM in the gain medium for various modulation depth and $r = 200$: (**a**) Steady-state pulse shapes after 500 000 cavity roundtrips, (**b**) corresponding power spectral densities, (**c**) time-bandwidth product and pulse width as a function of the modulation depth and (**d**) saturated net gain per round trip

[1]) and which is closely related to the occurence of a bump in the saturated gain (Fig. 9d). However, in the experiment, the side lobe is on the opposite side of the spectrum which we think is due to the unknown detuning in the experiment, which clearly influences the symmetry of the pulse.

In the active mode-locking experiments in [1] an AOM with a measured modulation depth of $M = 0.14$ was used. For the simulated pump parameter of $r = 200$, we obtain an average intracavity power of 25 W, which corresponds to an average intracavity intensity of 114 kW in the gain medium. In the experiment, we obtained a pulsewidth close to 5 ps and a time–bandwidth product of 0.8, respectively (Figs. 9a,c of [1]). In the simulation, we obtain for this parameter setting about 7 ps and the same time–bandwidth product of 0.8. Although the pulse spectra only agree qualitatively, which is probably due to the unknown detuning, we can trace back the characteristic occurrence of the side lobe in the spectrum to the influence of SPM in end-pumped lasers. The large time–bandwidth product is mainly due to the flat gain produced by SHB, not to a chirp on the pulse and therefore, cannot be compensated externally.

5 Passive mode locking with a saturable absorber and enhanced SHB

In this section, we investigate the effects of SHB on a passively mode-locked system. We consider as the mode-locking element a simple two-level broadband saturable absorber which is described by the following rate equation:

$$\frac{\partial q(T,t)}{\partial t} = -\frac{q - q_0}{T_A} - \frac{|A(T,t)|^2}{E_A}, \tag{19}$$

where q_0 are the non-saturated, but saturable losses per round trip, E_A is the saturation fluence of the absorber and T_A the absorber relaxation time. Assuming again small changes per pass, we can describe the action of the saturable absorber on the pulse per round trip as

$$A^q(T + T_R, t) = A(T,t)\exp[-q(T,t)], \tag{20}$$

where $q(T,t)$ is the solution of (19) in each round trip, assuming that the absorber recovers completely after each pulse since $T_A \ll T_R$. The parameters for the saturable absorber according to [1] are $q_0 = 0.0025$, $T_A = 3.8$ ps, $E_A = 5.1$ mJ/cm^2 for a spot size of $A_{\text{eff,A-FPSA}} = 2827$ μm^2 on the Antiresonant Fabry-Perot Saturable Absorber (A-FPSA). All the other laser parameters stay the same as in the actively mode-locked case. Simulations of the Nd:YLF laser for this parameter setting and for various pump parameters between $40 < r < 400$ were performed. The laser reached the steady state within a few thousand round trips. Figures 10a,b show the steady-state pulse shapes and spectra after 100 000 round trips. Again, we see that the pulse spectra are neither Gaussian-nor sech-shaped, resulting in small pre- and post-pedestals in the time domain. At low pumping, the modulation depth is again too small to lock the pronounced cw lasing spectrum due to SHB completely. The average intracavity power, pulsewidth and time–bandwidth product for the various pump parameters are shown in Fig. 10c. At low pumping levels, the time–bandwidth product is larger due to the lower pulse

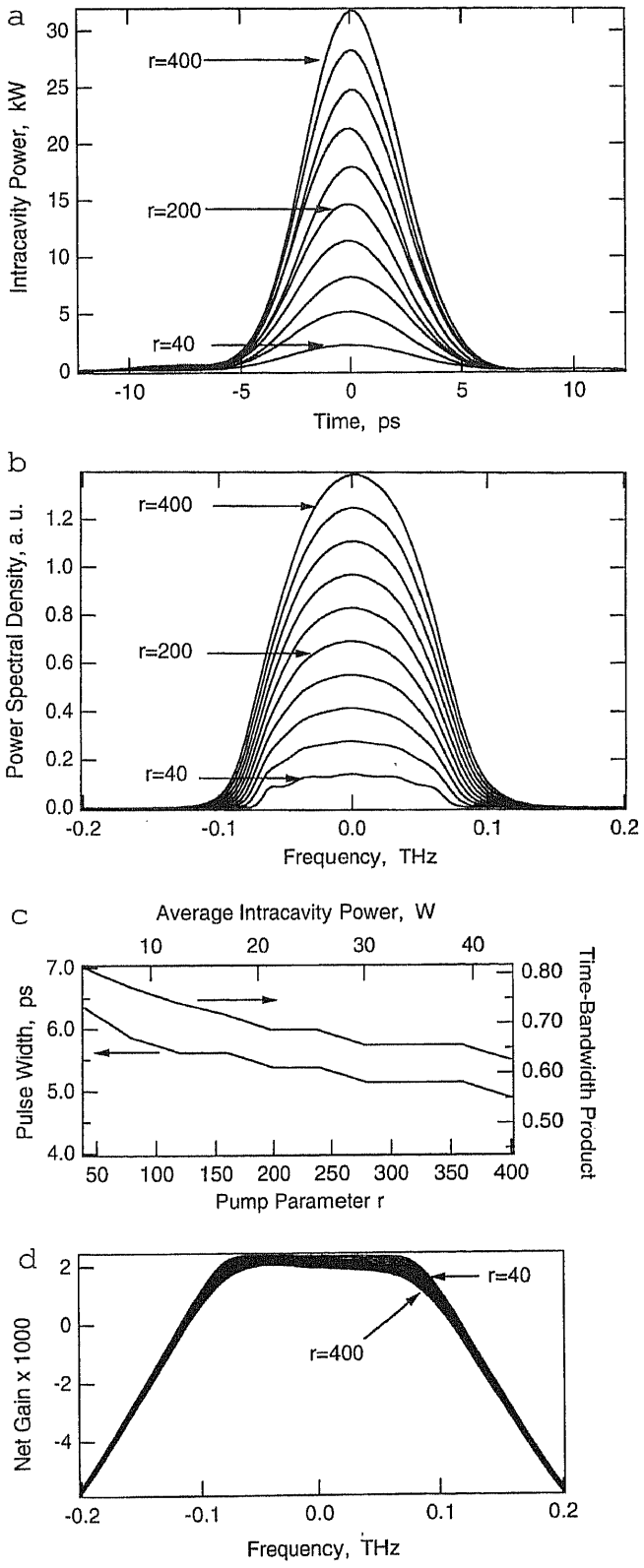

Fig. 10a–d. Simulation of an end-pumped Nd:YLF laser passively mode-locked by an A-FPSA with SPM in the gain medium for various pumping levels: (**a**) Steady-state pulse shapes after 100 000 cavity roundtrips. (**b**) Corresponding power spectral densities, (**c**) time–bandwidth product and pulse width as a function of the pump level r or average intracavity power and (**d**) saturated net gain per round trip

energy and therefore weaker saturation of the absorber. Despite the small modulation depth of the saturable absorber, the pulse shaping due to the passive mode-locker is stronger than the pulse shaping due to the active mode-locker, which results in somewhat shorter pulses of about 5 ps, compared to the 6 ps pulses achieved with the actively mode-locked laser in Sect. 2. The calculated pulsewidths of 4.9–6.3 ps agree rather well with the experimental values of 4–5 ps (Fig. 9a of [1]), especially as the pulsewidths are computed from the autocorrelation trace assuming a sech^2-shaped pulse and as we did not include the broadening of the gain bandwidth due to the heating of the crystal at strong pumping, investigated in [1]. This can also explain the difference of about 20% between the time–bandwidth products in the simulation of 0.65–0.75 and the experimental values of about 0.5–0.6. (Fig. 9c of [1]).

Due to the stronger pulse shaping by the passive absorber, the modulation due to the weak SPM in the gain medium is not important anymore. Simulation with and without SPM results in the same steady-state pulse shapes and spectra. Figure 10d shows the extracted net gain for the passively mode-locked laser. The net gain is again flattened by SHB in the mode-locked case. However, for increasing pump power, the flat part of the gain becomes narrower. This is due to the decreasing pulsewidth, because the region in the gain subjected to SHB is given by the overlap of the pulse with itself upon reflection at the end mirror. For a 5 ps pulse in Nd:YLF, the length of this overlap region is only $l_{\mathrm{SHB}} = 0.5$ mm, which accounts then only for one-ninth of the total gain length of 4.5 mm. For shorter pulses, the effects due to SHB are gradually vanishing, which results in a recovery of the Lorentzian lineshape of the saturated gain.

Simulation of the Nd:LSB laser results in a similar agreement between experiment and theory as for the Nd:YLF laser discussed here, but does not give any additional information.

6 Further pulse shortening by soliton-like pulse shaping

As we have seen from the experimental results in [1], lasers with a GE cavity exhibiting enhanced SHB give shorter pulses by a factor of about 3 due to SHB, in comparison to lasers with a GM cavity, while using the same modulation technique. This behavior is traced back to the flattening of the saturated gain due to SHB. The question that arises is whether we can use SHB beyond the experimental results obtained so far to achieve even shorter pulses, and whether we can improve on the time–bandwidth product of these lasers. External compression using dispersion only is not possible, since the large time–bandwidth product is not due to a chirp on the pulse. To improve on the time–bandwidth product, we can increase the SPM coefficient inside the cavity, while introducing negative GVD. This leads to the well-known soliton-like pulse shaping [19] resulting in sech-shaped pulses:

$$A(T,t) = \sqrt{\frac{W}{2\tau}}\,\mathrm{sech}\left(\frac{t}{\tau}\right)\exp\left(\mathrm{i}\Phi_0\frac{T}{T_R}\right),$$

with

$$\Phi_0 = \frac{\delta W}{4\tau} = \frac{|D|}{\tau^2}, \tag{21}$$

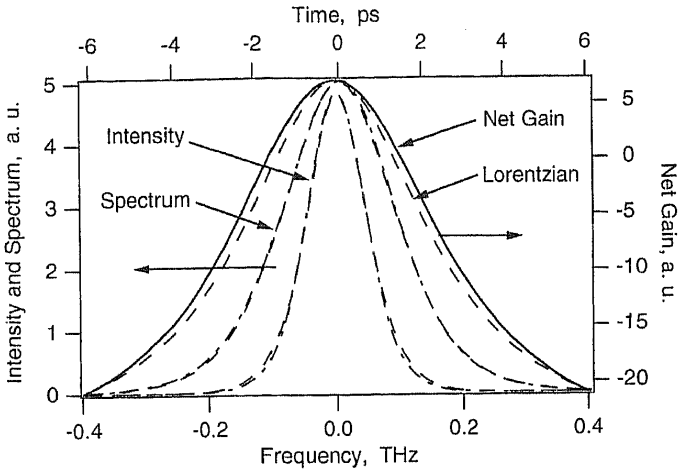

Fig. 11. Simulation of an end-pumped Nd:YLF laser passively mode-locked by an A-FPSA and soliton-like pulse shaping due to SPM and negative GVD in the gain medium. Steady-state intensity, power spectral density and saturated gain after 4000 cavity round trips. The *dashed line* shows the ideal Lorentzian lineshape of the Nd:YLF 1.047 μm lasing transition. The *dash-dotted lines* show the intensity profile and the spectrum of the pulse and the *dashed line* on top of these curves are the fits to a sech^2

where W is the pulse energy density in the medium causing the SPM, D the intracavity dispersion, Φ_0 is the phase shift of the soliton per roundtrip in the cavity and the FWHM pulse width is given by $\tau_{\mathrm{FWHM}} = 1.76\,\tau$. We make the soliton-like pulse shaping as strong as possible, without leaving the regime of small changes per pass. Therefore, we determine the SPM coefficient and the dispersion so that the phase shift of the soliton is roughly 15% per round trip, i.e., $\Phi_0 = 0.15$. Thus, the soliton-like pulse shaping is at least a hundred times stronger than the pulse shaping due to gain filtering or the saturable absorber. For the typical pulse energy of 80 nJ in the Nd:YLF laser focused to a spot size $A_{\mathrm{eff,SPM}} = \pi \times 30 \times 30\ \mu\mathrm{m}^2$ in a highly nonlinear glass and for a desired pulse width of 2 ps, we obtain from (26) $D = -0.2\ \mathrm{ps}^2$ and $\delta = 2\ \mathrm{cm}^2/\mathrm{GW}$, which can be realized by a Gires-Tournois Interferometer (GTI) and by focusing into a highly nonlinear glass like SF10. However, this alone does not lead to a stable pulse formation. Only if we additionally increase the amount of saturable absorption we can obtain stable pulses. Thus, Fig. 11 shows the results of the simulation with the above values for SPM and GVD, and with the other laser parameters chosen as $q_0 = 0.01$, $T_A = 3.8$ ps, $E_A = 0.7\ \mathrm{mJ/cm}^2$, $l = 0.028$, $r = 100$. The higher saturable absorption also necessitates additional intracavity losses, leading to a new increased total loss value and a reduced pump parameter value. The reduction in the saturation energy can easily be achieved by reducing the top reflectivity of the A-FPSA [20]. Thus, the parameters used in the simulation are realistic. The other laser parameters stay the same. Figure 11 shows the new steady-state solution in the time and frequency domain and the saturated gain. We obtain an almost transform-limited 1.7 ps pulse with a time–bandwidth product of 0.34. The small deviation from the transform limit is due to the fact that we couple the pulse out of the cavity after passing the SPM section. The pulse energy in the steady state is 88 nJ. The pulse shape and the spectrum fit very well to a sech^2 (Fig. 11). Due to the shorter pulse, the overlap region in the gain is reduced to 1/20 of the gain length. This reduces the influence of SHB when the pulse reaches the steady state and leads to an almost perfect recovery of the Lorentzian-shaped saturated gain, which helps to improve the time–bandwidth product.

Simulation of the Nd:LSB laser with the same absorber parameters, but reduced values for GVD and SPM, results in pulses as short as 400 fs, even though we used an absorber which recovers only after 3.8 ps. This result was well explained in a previous publication [21] showing that, with soliton-like pulse shaping, the pulsewidth is not limited to the recovery time of the absorber. Here, we obtain pulses almost ten times shorter than the absorber recovery time.

7 Conclusion

We have studied numerically the influence of SHB on end-pumped solid-state lasers. The simple laser model developed here allows for an efficient simulation of the laser dynamics by making extensive use of the FFT. The laser parameters used for the simulations were independently measured and not used to fit experimental data. The results obtained with respect to the cw running and cw mode-locked behavior fit the experimental results obtained in [1] very well within the measurement errors already involved with parameter extraction. We could verify and make plausible that the spacing of the cw lasing modes is approximately given by the length of the gain medium which maximizes mutually the gain for the running modes for a large parameter regime regarding absorption depth of the pump transition and actual length of the gain medium.

Furthermore, we have shown that the large time–bandwidth product usually obtained in end-pumped solid-state lasers is due to the square-shaped pulse spectra produced by the flattened gain via SHB. This also leads to pedestals or wings of the pulse in the time domain. Using soliton-like pulse shaping, we demonstrated by numerical simulation that the time–bandwidth product can be improved drastically and that further pulse shortening can be achieved in end-pumped lasers. Thus, we predict the possibility of a 2 ps Nd:YLF and a 400 fs Nd:LSB laser with this technique.

Appendix: Numerical implementation of the optical gain deformed by SHB

For the numerical simulation, we have to simulate the laser up to a million of round trips to prove that a stationary state is reached. Therefore, we need a highly efficient method for the evaluation of the gain according to (11). This is achieved by extensive use of FFT.

For the function occurring in the denominator of the gain in (11), we can write

$$8 \sum_m L(\omega_0 - \omega_m) \frac{|A_m|^2}{I_L} \sin^2(k_m z) = S(0) - \mathrm{Re}\{S(z) \exp(\mathrm{i}2k_{0g}z)\} \tag{A1}$$

where we have introduced the saturation function

$$S(z) = 4 \sum_{m=0}^{N} L(\omega_0 - \omega_m) \frac{|A_m|^2}{I_L} \exp[\mathrm{i}2(k_m - k_{0g})z], \quad \text{(A2)}$$

with the mode wave numbers according to (2b) and the wave number of the center mode $k_{0g} = 2\pi/\lambda\, n_r$ in the gain medium. Since the Lorentzian profile determines the spectral width of the laser, the saturation function is a slowly varying function over the wavelength in the gain medium as long as $2\pi f_g/\omega_0 \ll 1$ which is for Nd:YLF $2\pi f_g/\omega_0 = 4 \times 10^{-4}$. With the saturation function (A2), we can write for the gain

$$G(\omega_n) = \frac{rlL(\omega_0 - \omega_n)\alpha}{1 - \mathrm{e}^{-\alpha l_g}} \int_0^{l_g} \frac{1 - \mathrm{Re}\{\exp[\mathrm{i}2(k_n - k_{0g})z] \exp(\mathrm{i}2k_{0g}z)\}}{1 + S(0) - \mathrm{Re}\{S(z)\exp(\mathrm{i}2k_{0g}z)\}} \mathrm{e}^{-\alpha z}\, dz\,. \quad \text{(A3)}$$

We can divide the integration in (A3) into intervals over one wavelength in the gain medium. Since the saturation function is slowly varying over a wavelength and we are only interested in the gain over a spectral width on the order of the gain bandwidth, we can pull out the slowly varying terms from the individual integrals and obtain

$$G(\omega_n) = \frac{rlL(\Omega - \omega_n)}{1 - \mathrm{e}^{-\alpha l_g}} \frac{\alpha}{2k_{0g}} \sum_{m=0}^{M} \mathrm{e}^{-\alpha m \Delta z} \times \left[\frac{1}{\sqrt{[1 + S(0)]^2 - |S(m\Delta z)|^2}} + \left(1 - \frac{[1 + S(0)]}{\sqrt{[1 + S(0)]^2 - |S(m\Delta z)|^2}}\right) \times \mathrm{Re}\left\{ \frac{S(m\Delta z)^*}{|S(m\Delta z)|^2} \exp[\mathrm{i}2(k_n - k_{0g})m\Delta z] \right\} \right], \quad \text{(A4)}$$

with $\Delta z = \pi/k_{0g}$ and where we have used the integral

$$\frac{1}{2\pi} \int_0^{2\pi} \frac{\exp(\mathrm{i}\varphi)}{a + b\cos\varphi}\, d\varphi = \frac{1}{b}\left(1 - \frac{a}{\sqrt{a^2 - b^2}}\right). \quad \text{(A5)}$$

The sum in (A4) can also be evaluated using the FFT if we rewrite it by evaluating the saturation function at the discrete points $\Delta z_g = \pi/N\Delta k_g$ for $0 < m < M_g$, with $M_g = l_g/\Delta z_g$, N is the number of points used for the FFT. Then, we can use the FFT for the same number of modes and space points for the evaluation of (A4) and (A5). For the simulation of the cw lasing pattern we used $N = 2^{13}$. This choice results in $M_g = 90$ points in the gain region, resolving the slowly varying saturation function very well.

For the simulation of the mode-locked laser we used $N = 2^{10}$. Since the steady-state pulses are shorter than the gain length, we did not have to resolve the field over the whole cavity: the gain region is in principle enough. Therefore, we only simulated every 16 th mode, which leads to a good resolution of the pulse in the time and frequency domain. The spectra and pulse shapes (Figs. 7–11) show one-tenth of the actually simulated region in the frequency and time domain. With this choice, we have 122 points in the gain medium to resolve the slowly varying saturation function.

References

1. B. Braun, K.J. Weingarten, F. X. Kärtner, U. Keller: Appl. Phys. B **61**, 429 (1995)
2. C. L. Tang, H. Statz, G. DeMars: J. Appl. Phys. **34**, 2289 (1963)
3. M. Sargent: Appl. Phys. **9**, 127 (1976)
4. J. J. Zayhowski: Opt. Lett. **15**, 431 (1990)
5. G. J. Kintz, T. Baer: IEEE J. QE-**26**, 1457 (1990)
6. M. Sargent, M. O. Scully, J. W. E. Lamb: *Laser Physics* (Addison-Wesley Reading 1974)
7. C. J. Flood, D. R. Walker, H. M. v. Driel: Opt. Lett. **20**, 58 (1995)
8. M. S. Stix, E. P. Ippen: IEEE J. QE-**19**, 520 (1983)
9. H. Fu, H. Haken: Phys. Rev. A **43**, 2446 (1991)
10. H. Haken, H. Sauermann: Z. Phys. **173**, 261 (1963)
11. H. Haken, H. Sauermann: Z. Phys. **176**, 47 (1963)
12. H. Haken: *Laser Theory*, Encyclopedia of Physics, Vol. XXV/2c (Springer, Berlin, Heidelberg 1970)
13. H. Haken: *Advanced Synergetics*, Springer Ser. Syn., Vol. 20 (Springer, Berlin, Heidelberg 1983)
14. L. O. Chua: *Computer Aided Analysis of Electronic Circuits: Algorithms and Computational Techniques* (Prentice-Hall, Englewood Cliffs, NJ 1975)
15. D. J. Kuizenga, A. E. Siegman: IEEE J. QE-**6**, 694 (1970)
16. H. A. Haus: IEEE J. QE-**11**, 323 (1975)
17. J. Sweetser, T. J. Dunn, I. A. Walmsley: Opt. Commun. **97**, 379 (1993)
18. H. A. Haus, Y. Silberberg: IEEE J. QE-**22**, 325 (1986)
19. O. E. Martinez, R. L. Fork, J. P. Gordon: J. Opt. Soc. Am. B **2**, 753 (1985)
20. L. R. Brovelli, U. Keller, T. H. Chiu: J. Opt. Soc. Am. B **12**, 311 (1995)
21. F. X. Kärtner, U. Keller: Opt. Lett. **20**, 16 (1995)